Calculated Structures and Electronic Absorption Spectroscopy for Magnesium Phthalocyanine and Its Anion Radical

Marshall G. Cory, Hiroaki Hirose, and Michael C. Zerner*

Quantum Theory Project, University of Florida, Gainesville, Florida 32611

Received January 18, 1995[⊗]

Structures are calculated for magnesium phthalocyanine (MgPc) and its radical anion doublet ($MgPc^-$), using both *ab-initio* (6-31G**) and semiempirical (INDO/1) self-consistent field approaches. The anion is first-order Jahn–Teller distorted, and the various distortions that are possible are examined. The electronic absorption spectra of both molecular species and the effect that varying the degree of distortion has on the computed anion spectrum are discussed. These results suggest that the four-orbital model often applied to porphyrin systems in interpreting the low-energy spectrum is incomplete for the anion case. We further conclude that the Jahn–Teller distortions calculated by either *ab-initio* or semiempirical models may be too great.

Introduction

Recent articles[1-4] concerning the experimental UV–vis spectral properties of the radical anion of metal phthalocyanines and their interpretation have spurred our interest in the calculation of such properties. In this work we obtain calculated UV–vis absorption spectra for both magnesium phthalocyanine (MgPc) and its anion radical. Workers in this area have explained the spectral features of the phthalocyanines using the four-orbital model of Gouterman.[5] It seems reasonable that this model can be applied to the electrically neutral phthalocyanines, as the principal structural features present in porphyrin, the species for which this model was developed, are also present in phthalocyanine. Phthalocyanine, like porphyrin, can be likened to 16-member conjugated macrocycles and, usually, possesses a 2- or 4-fold principal symmetry axis. The four-orbital model does, indeed, explain many of the features of the low-energy $\pi \rightarrow \pi^*$ transitions localized to the porphyrin-like macrocycle. It is not obvious that this elegantly simple model can be applied to anionic structures, where the reducing electron occupies the lowest energy π^* orbital of the neutral species. We will address the applicability of this model to these systems through the interpretation of our calculated spectra. We also compare our calculated results to those obtained experimentally in an attempt to better understand the observed spectrum.

Before a spectrum can be calculated, a "reasonably" good structure must be obtained either by direct experimental observation or, when such information is not available, by computational techniques. In this paper we will compare the computed spectra of four quantum chemically optimized structures to spectra acquired experimentally, as the calculated spectrum, especially of the anion, is remarkably sensitive to the geometry. From our results we comment on the ability of theory to produce good structures and to predict the UV–vis spectral properties.

Computational Methods

Structures. The initial MgPc structure was obtained through the use of a CAChe workstation.[6] The neutral structure was generated and then refined using a modified MM2 force field[7] available with the CAChe system. This classically optimized structure served as the starting point for the quantum chemical structural optimization.

For the *ab-initio* structural optimizations we used the GAMESS[8] program package. We optimized both the neutral and the radical anion at the restricted Hartree–Fock[9] (RHF) and restricted open-shell Hartree–Fock[10-15] (ROHF) self-consistent field[16] (SCF) levels, respectively, using a 6-31G** basis set.[17-20] At the semiempirical level of approximation we used the ZINDO[21-30] program package to obtain the optimized structures. Once again, both structures were optimized at the SCF level using RHF for the neutral and ROHF[31] for the doublet

[⊗] Abstract published in *Advance ACS Abstracts,* May 1, 1995.

(1) Golovin, N. M.; Seymour, P.; Fu, K.; Lever, A. B. P. *Inorg. Chem.* **1990**, *29*, 1719.
(2) Kobayashi, N.; Lam, H.; Nevin, W. A.; Janda, P.; Leznoff, C. C.; Lever, A. B. P. *Inorg. Chem.* **1990**, *29*, 3415.
(3) Kadish, K. M.; Franzen, M. M.; Han, B. C.; Araullo-McAdems, C.; Sazou, D. *J. Am. Chem. Soc.* **1991**, *113*, 512.
(4) Mack, J.; Kirkby, S.; Ough, E. A.; Stillman, M. J. *Inorg. Chem.* **1992**, *31*, 1717.
(5) Gouterman, M. *The Porphyrins, Volume III*; Academic Press: New York, 1978.
(6) CAChe Scientific, P.O. Box 500, Mail Station 13-400 Beaverton, OR 97077.
(7) Purvis, G. D., III. *Comp. Aided Mol. Des.* **1991**, *5*, 55.
(8) Schmidt, M. W.; Baldridge, K. K.; Boatz, J. A.; Jensen, J. H.; Koseki, S.; Gordon, M. S.; Nguyen, K. A.; Windus, T. L.; Elbert, S. T. *QCPE Bull.* **1990**, *10*, 52.
(9) Roothaan, C. C. J. *Rev. Mod. Phys.* **1951**, *23*, 69.
(10) McWeeny, R.; Diercksen, G. *J. Chem. Phys.* **1968**, *49*, 4852.
(11) Guest, M. F.; Saunders, V. R. *Mol. Phys.* **1968**, *28*, 819.
(12) Binkley, J. S.; Pople, J. A.; Dobosh, P. A. *Mol. Phys.* **1974**, *28*, 1423.
(13) Davidson, E. R. *Chem. Phys. Lett.* **1973**, *21*, 565.
(14) Faegri, K.; Manne, R. *Mol. Phys.* **1976**, *31*, 1037.
(15) Hsu, H.; Davidson, E. R.; Pitzer, R. M. *J. Chem. Phys.* **1976**, *65*, 609.
(16) Szabo, A.; Ostlund, N. S. *Modern Quantum Chemistry. Introduction to Advanced Electronic Structure Theory*; McGraw-Hill: New York, 1989.
(17) Ditchfield, R.; Hehre, W. J.; Pople, J. A. *J. Chem. Phys.* **1971**, *54*, 724.
(18) Hehre, W. J.; Ditchfield, R.; Pople, J. A. *J. Chem. Phys.* **1972**, *56*, 2257.
(19) Francl, M.; Pietro, W. J.; Hehre, W. J.; Binkley, J. S.; Gordon, M. S.; DeFrees, D. J.; Pople, J. A. *J. Chem. Phys.* **1982**, *77*, 3654.
(20) Davidson, E. R.; Feller, D. *Chem. Rev.* **1986**, *86*, 681.
(21) Ridley, J. E.; Zerner, M. C. *Theor. Chim. Acta* **1973**, *32*, 111.
(22) Zerner, M. C.; Loew, G. H.; Kirchner, R. F.; Mueller-Westerhoff, U. T. *J. Am. Chem. Soc.* **1980**, *102*, 589.
(23) Ridley, J. E.; Zerner, M. C. *Theor. Chim. Acta* **1976**, *42*, 223.
(24) Bacon, A.; Zerner, M. C. *Theor. Chim. Acta* **1979**, *53*, 21.
(25) Head, J.; Zerner, M. C. *Chem. Phys. Lett.* **1985**, *122*, 264.
(26) Head, J.; Zerner, M. C. *Chem. Phys. Lett.* **1986**, *131*, 359.
(27) Anderson, W.; Edwards, W. D.; Zerner, M. C. *Inorg. Chem.* **1986**, *25*, 2728.
(28) Edwards, W. D.; Zerner, M. C. *Theor. Chim. Acta* **1987**, *72*, 347.
(29) Kotzian, M.; Roesch, N.; Zerner, M. C. *Theor. Chim. Acta* **1992**, *81*, 201.
(30) Kotzian, M.; Roesch, N.; Zerner, M. C. *Int. J. Quant. Chem.* **1991**, 545.

0020-1669/95/1334-2969$09.00/0

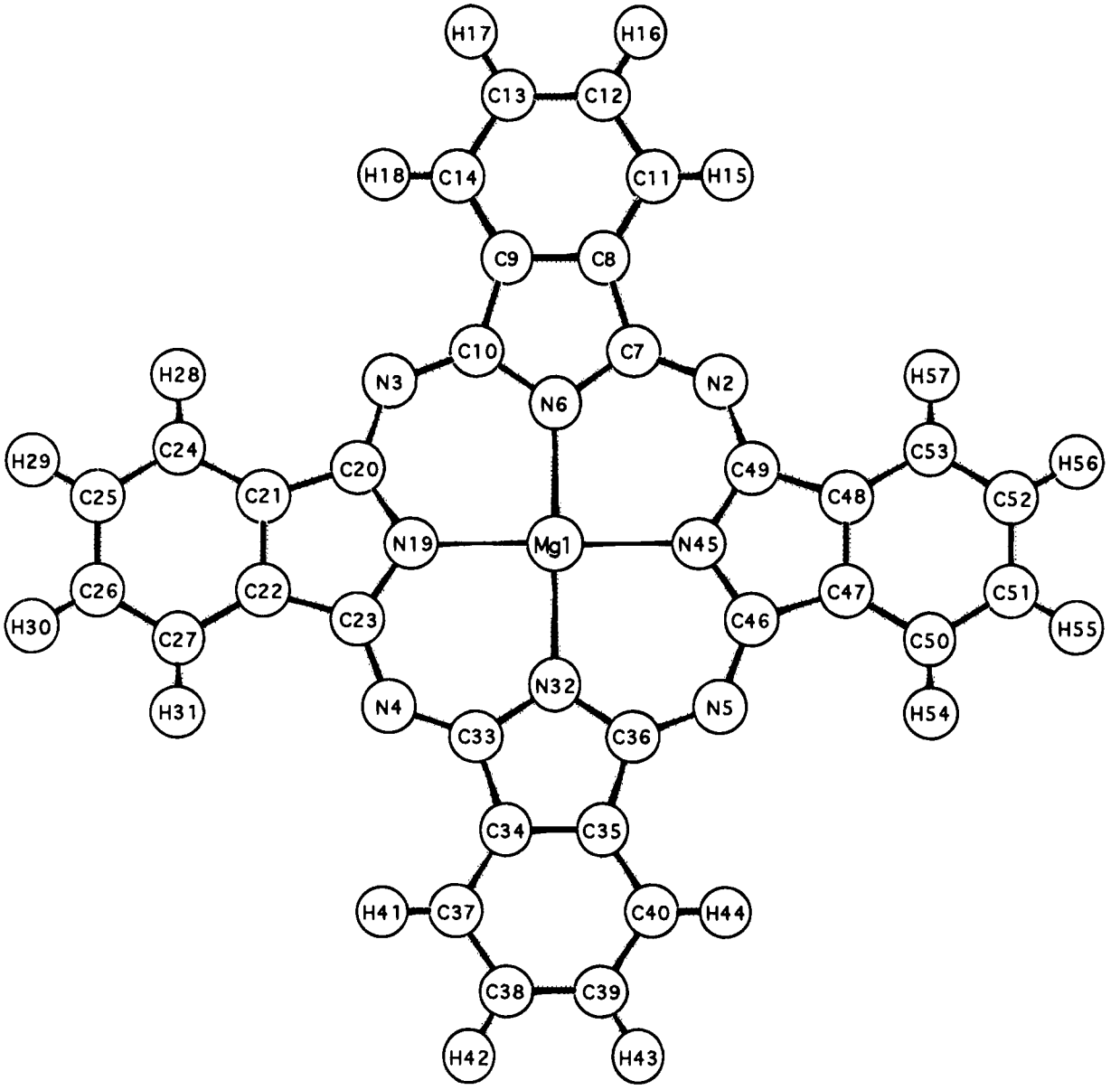

Figure 1. Magnesium phthalocyanine and the atomic numbering scheme used for the tables and text. The elongation for the anion is along the *y* axis, which is defined by atoms 6 and 32. The *z* axis is perpendicular to the molecular plane.

anion. These SCF optimizations were carried out at the intermediate neglect of differential overlap/1[32] (INDO/1) level of approximation.

In both cases, *ab-initio* and semiempirical models, it was assumed that the neutral structure had D_{4h} symmetry. Adding an electron to the neutral D_{4h} species, to form the initial structure of the radical anion, leads to the single unpaired electron populating a degenerate $e_g(\pi^*)$ molecular orbital. We then optimized the anion radical in the following two ways: (1) one electron in one of the two $e_g(\pi^*)$ orbitals, allowing the molecule to Jahn–Teller[33] distort into two possible structures both with D_{2h} symmetry, and (2) one electron averaged over the two $e_g(\pi^*)$ orbitals. This latter averaging method maintains the D_{4h} symmetry of the neutral species while relaxing the structure. We take the difference in energies between (1) and (2) to be the Jahn–Teller distortion energy.

Electronic Spectra. Having obtained the optimized MgPc and $MgPc^-$ structures via the above described methods, we then utilized them to obtain the calculated UV–vis absorption spectra, using the ZINDO program package. The spectroscopic INDO Hamiltonian (INDO/S)[21,22] was used to generate a set of molecular orbitals (MO) which were then used to construct the multielectron basis for a singles-only configuration interaction (CIS) calculation[34] to determine the state energies and absorption intensities. The INDO/S method has been specifically parametrized to yield good spectroscopic transition energies at the CIS level.

For the neutral species the active orbitals in the CI were the 50 lowest energy virtual molecular orbitals and the 50 highest energy occupied molecular orbitals. This same active space was spanned for the CIS calculation of the anion. The active space may be adjusted up or down by one orbital as needed to prevent the splitting of a degenerate MO level or, in the case of the D_{2h} structures, those orbitals that would be degenerate if the structure were of D_{4h} symmetry.

Results

The atomic numbering scheme used to label the symmetry-unique bond lengths and bond angles is given in Figure 1. Their calculated values, for both optimization methods and both molecular species, can be found in Tables 1 and 2.

The calculated UV–vis absorption spectra for the neutral species are given in Table 5 for the INDO/1-optimized structure

(31) Edwards, W. D.; Zerner, M. C. *Theor. Chim. Acta* **1987**, *72*, 347.
(32) Pople, J. A.; Beveridge, D.; Dobash, P. A. *Chem. Phys.* **1967**, *47*, 2026.
(33) Bersuker, I. B. *The Jahn Teller Effects and Vibronic Interactions in Modern Chemistry*; Plenum Press: New York, 1984.
(34) In *Methods of Electronic Structure Theory, Volume IV*; Schaefer, H. F., Ed.; Plenum Press: New York, 1984.

Table 1. Symmetry-Unique Bond Lengths (Å) for MgPc and $MgPc^-$

	MgPc [D_{4h}]		$MgPc^-$ [D_{2h}]	
atoms[a]	6-31G**	INDO/1	6-31G**	INDO/1
1−6	1.995	2.098	1.993	2.094
1−19			2.008	2.109
3−10	1.317	1.353	1.291	1.339
3−20			1.356	1.347
6−10	1.351	1.381	1.362	1.380
8−9	1.393	1.429	1.389	1.428
9−10	1.459	1.456	1.476	1.462
9−14	1.390	1.401	1.386	1.398
12−13	1.403	1.401	1.397	1.398
13−14	1.378	1.391	1.383	1.394
13−17	1.076	1.096	1.077	1.097
14−18	1.074	1.096	1.075	1.096
19−20			1.351	1.380
20−21			1.427	1.439
21−22			1.409	1.439
21−24			1.406	1.410
24−25			1.366	1.383
24−28			1.075	1.097
25−26			1.420	1.411
25−29			1.077	1.097

[a] See Figure 1.

Table 2. Symmetry-Unique Bond Angles (deg) for MgPc and $MgPc^-$

	MgPc [D_{4h}]		$MgPc^-$ [D_{2h}]	
atoms[a]	6-31G**	INDO/1	6-31G**	INDO/1
1−6−10	124.7	124.2	124.6	124.0
1−19−20			124.8	124.1
3−10−6	126.6	126.1	128.9	127.1
3−10−9	124.1	126.8	123.4	128.7
3−20−19			127.1	126.1
3−20−21			124.5	126.9
6−1−19	90.0	90.0	90.0	90.0
6−1−45			90.0	90.0
6−10−9	108.3	107.1	107.7	106.6
7−2−49			124.6	128.7
7−6−10	110.5	111.7	110.9	112.0
8−9−10	106.5	107.1	106.8	107.4
9−8−11	121.2	120.8	121.2	120.0
9−14−13	117.6	118.9	117.8	119.3
9−14−18	120.8	120.5	120.6	120.6
10−3−20	125.3	129.4	124.6	128.7
10−9−14	132.4	132.8	132.0	132.7
12−13−14	121.2	121.0	121.0	120.8
14−13−17	119.7	119.8	119.7	119.8
19−20−21			108.4	107.0
20−19−23			110.3	111.8
20−21−22			106.4	107.1
20−21−24			133.1	133.4
21−22−27			120.4	119.5
21−24−25			118.4	119.7
21−24−28			120.3	120.0
24−25−26			121.2	120.8
24−25−29			119.9	120.2

[a] See Figure 1.

and in Table 6 for the *ab-initio* SCF optimized structure; the calculated stick spectra were also fitted to Lorentzian distribution functions and plotted. (See the Appendix for a complete description of the Lorentzian function used.) These plots can be found in Figure 2. For the radical anion the calculated UV−vis absorption spectrum of the INDO/1 structure can be found in Table 7 and the results for the *ab-initio* SCF structure can be found in Table 8. Their Lorentzian distributions are plotted in Figure 5.

Those molecular orbitals which participate in the description of the electronic excitation spectra are ordered by energy and labeled by symmetry in Figure 3*a* for the INDO/1-optimized neutral structure and in Figure 3*b* the anionic INDO/1 structure is likewise labeled. Finally, Tables 1 and 2, and Figure 1 list and show how the optimized anionic structures Jahn−Teller distort.

Discussion

Neutral MgPc (D_{4h}). The vapor-phase absorption spectrum of neutral MgPc has been reported many times.[35,36] The five distinct peaks between 800 and 200 *nm* have been labeled as **Q**, **B**, **N**, **L**, and **C**, the same description used for porphyrin spectra.[35] We adhere to this convention while explaining our results. The experimentally observed bands, as well as those calculated, can be found in Table 3. Our assignment of **Q**, $\mathbf{B}_1$, $\mathbf{B}_2$, **N**, **L**, and **C** is somewhat arbitrary. We assign these labels to the six lowest energy E_u bands of observable intensity for both the INDO/1 structure and the *ab-initio* structure. For both calculated structures the band labeled **B** is composed of two calculated E_u transitions. For both structures these two bands lie too close in energy to be readily distinguishable experimentally; see Figures 2 and 6*a*. In the literature these have been noted, and labeled, as $\mathbf{B}_1$ and $\mathbf{B}_2$. The split **B** band is not resolved in the gas-phase spectrum of ref 35 but is seen in the MCD spectrum of ref 4. For the most part the E_u bands are described by excitations localized to the macrocycle. It is then interesting to note the differences in the calculated E_u bands between the two optimized structures and correlate these observations with the main structural difference. Although there are several, the principal ones are the Mg to N bond distance, 2.098 Å vs 1.993 Å, and the circumference around the macrocycle, 21.872 Å vs 21.344 Å for the INDO/1 and *ab-initio* structures, respectively. Although we have not been able to locate an experimental Mg−N bond length in MgPc, Mg−N bond lengths in porphyrins and chlorins are generally found to be between 2.05 and 2.13 Å. The effect of this upon the calculated spectrum is observed in Figure 2 and in Tables 5 and 6. We observe that the calculated excitation energies remain relatively constant between the two structures used in their computation, although there is a small red shift for the larger INDO/1 structure, while the computed oscillator strengths differ significantly; that is, the band centers appear insensitive to small structural changes, while oscillator strengths tend to be more sensitive.

As can be seen in Table 3 there is some discrepancy between the reported experimental spectra; this difference is larger than might easily be explained from solvent shifts. The positions of the bands of the solvated spectrum were obtained via deconvolution calculations.[35] Our quantum chemical calculations are best compared with the observed vapor-phase spectrum.

Most of the intensity in both porphyrins and phthalocyanines derives from the four-orbital model, leading to four excitations: $1a_{1u} \rightarrow 1e_g^*(xz)$, $1a_{2u} \rightarrow 1e_g^*(xz)$, $1a_{1u} \rightarrow 1e_g^*(yz)$, and $1a_{2u} \rightarrow 1e_g^*(yz)$; see Figure 3. For magnesium porphyrin the $1a_{1u}$ and $1a_{2u}$ molecular orbitals are calculated to be nearly degenerate as are the excitations from these orbitals into $1e_g^*$. These strongly allowed excitations mix through the configuration interaction treatment. For the lower energy transition, **Q** band, the intensities cancel, and for the higher energy **B** band, they reinforce. In the magnesium porphyrin INDO/S−CIS calculation the **Q** band[37] is composed of 60% $1a_{1u} \rightarrow 1e_g^*$ and 40% $1a_{2u} \rightarrow 1e_g^*$, and the **B** band is composed of the same two one-

(35) Gouterman, M. *J. Mol. Spectrosc.* **1970**, *33*, 292.
(36) Ough, E.; Nyokong, T.; Creber, K. A. M.; Stillman, M. J. *Inorg. Chem.* **1988**, *27*, 2724.
(37) Results for an INDO/S-CIS calculation using a INDO/1-optimized structure.

Table 3. Experimentally Observed and Calculated Spectral Data for MgPc

	bands ($nm/10^3$ cm^{-1})						
spectrum	Q	B[a]	B_1	B_2	N	L	C
vapor[b]	663/15.1	330/30.3			280/35.7	242/41.3	219/45.5
soln[c]	670/14.9		361/27.7	325/30.8	338/29.6	281/35.6	246/40.7
INDO/1	730/13.7		325/30.8	316/32.1	288/34.7	239/41.9	223/44.9
6-31G**	725/13.8		305/32.8	303/33.1	257/34.4	236/42.0	221/45.2

[a] The splitting of the B band was not observed in the gas-phase spectrum. [b] Reference 35. [c] Reference 4.

Table 4. Lettered E_u States of Neutral D_{4h} MgPc in Terms of Orbital Excitations (energy, 10^3 cm^{-1})

	INDO/1		6-31G**	
band	ene/osc	% excitation	ene/osc	% excitation
Q	13.7/1.59	90 $1a_{1u} \rightarrow 1e_g^*$	13.8/1.55	90 $1a_{1u} \rightarrow 1e_g^*$
		7 $1a_{2u} \rightarrow 1e_g^*$		6 $1a_{2u} \rightarrow 1e_g^*$
	28.8/0.02	95 $1a_{1u} \rightarrow 2e_g^*$	28.6/0.04	95 $1a_{1u} \rightarrow 2e_g^*$
B_1	30.8/1.10	44 $1b_{1u} \rightarrow 1e_g^*$	32.8/1.29	46 $1b_{1u} \rightarrow 1e_g^*$
		27 $2a_{2u} \rightarrow 1e_g^*$		25 $2a_{2u} \rightarrow 1e_g^*$
		12 $1a_{2u} \rightarrow 1e_g^*$		11 $1a_{2u} \rightarrow 1e_g^*$
B_2	32.1/3.33	63 $1a_{2u} \rightarrow 1e_g^*$	33.1/1.69	32 $1a_{2u} \rightarrow 1e_g^*$
		18 $1b_{1u} \rightarrow 1e_g^*$		28 $1a_{1u} \rightarrow 3e_g^*$
		6 $1a_{1u} \rightarrow 3e_g^*$		20 $1b_{1u} \rightarrow 1e_g^*$
N	34.7/0.70	44 $1a_{1u} \rightarrow 3e_g^*$	34.4/1.80	40 $1a_{2u} \rightarrow 1e_g^*$
		18 $2a_{2u} \rightarrow 1e_g^*$		22 $1a_{1u} \rightarrow 3e_g^*$
		11 $1a_{2u} \rightarrow 1e_g^*$		
	36.8/0.08	41 $1a_{1u} \rightarrow 3e_g^*$	36.7/0.00	36 $1a_{1u} \rightarrow 3e_g^*$
		23 $2a_{2n} \rightarrow 1e_g^*$		25 $1b_{2u} \rightarrow 1e_g^*$
		13 $1b_{2u} \rightarrow 1e_g^*$		
		10 $1b_{2u} \rightarrow 1e_g^*$		
	38.1/0.13	47 $1b_{2u} \rightarrow 1e_g^*$	38.9/0.22	52 $2a_{2u} \rightarrow 1e_g^*$
		19 $2a_{2u} \rightarrow 1e_g^*$		23 $1b_{1u} \rightarrow 1e_g^*$
		11 $1b_{1u} \rightarrow 1e_g^*$		10 $1b_{2u} \rightarrow 1e_g^*$
L	41.9/0.50	34 $1b_{2u} \rightarrow 1e_g^*$	42.0/0.20	46 $1b_{2u} \rightarrow 1e_g^*$
		33 $2a_{1u} \rightarrow 1e_g^*$		19 $2a_{1u} \rightarrow 1e_g^*$
	42.9/0.04	84 $1a_{1u} \rightarrow 4e_g^*$	42.8/0.06	82 $1a_{1u} \rightarrow 4e_g^*$
C	44.9/1.37	44 $3a_{1u} \rightarrow 1e_g^*$	45.2/1.05	48 $2a_{1u} \rightarrow 1e_g^*$
		11 $1e_g \rightarrow 1b_{1u}^*$		8 $1e_g \rightarrow 1b_{1u}^*$
		11 $1e_g \rightarrow 1a_{2u}^*$		8 $1e_g \rightarrow 1a_{2u}^*$
	47.7/0.26	63 $1e_g \rightarrow 1b_{2u}^*$	48.8/0.05	40 $1e_g \rightarrow 1b_{2u}^*$
	49.4/0.22	69 $1a_{2u} \rightarrow 2e_g^*$	49.9/0.08	26 $1a_{2u} \rightarrow 2e_g^*$
				18 $1a_{1u} \rightarrow 5e_g^*$
				12 $2e_g \rightarrow 1b_{2u}^*$

Table 5. Electronic Excitation Spectral Data for the Neutral MgPc INDO/1-Optimized Structure

		transition energy (10^3 cm^{-1})	
state	symmetry[a]	calcd	obsd[b]
1	A_{1g}		
2, 3	E_u	13.7 (1.5890)[c] Q[d]	15.1 [15.9, 16.9][e]
4	B_{2g}	23.4	
5	A_{1g}	25.6	
6	A_{2g}	27.5	
7, 8	E_u	28.8 (0.0212)	
9, 10	E_g	29.3	
11	A_{2u}	29.9 (0.0331)	
12	A_{2g}	30.3[f]	
14, 15	E_u	30.8 (1.1010) B_1	30.3[g]
16	A_{2g}	31.1[h]	
17, 18	E_u	32.1 (3.3298) B_2	
21	B_{2g}	34.7	
24, 25	E_u	34.7 (0.7004) N	35.7
31, 32	E_u	36.8 (0.0766)	
38, 39	E_u	38.1 (0.1286)	
43, 44	E_u	41.9 (0.5026) L	41.3
47, 48	E_u	42.9 (0.0432)	
52, 53	E_u	44.9 (1.3680) C	45.5

[a] (x, y) transforms as e_u and (z) transforms as a_{2u} in D_{4h}. [b] From ref 35. [c] Values in parentheses are calculated oscillator strengths. [d] Spectroscopic labels for the degenerate transitions, Q, B_2, B_2, N, L, and C. See ref 35. [e] Vibrational fine structure; see text, as well as refs 4 and 35. [f] Beyond 30 300 cm^{-1} only states with calculated oscillator strengths are reported. [g] The absorption is broad (see ref 4) and is assigned to calculated states (7−18); see also Figure 2a. [h] The only state below 50 000 cm^{-1} with significant charge transfer character; 50% Pc → Mg ($\pi \rightarrow \pi^*$).

electron orbital excitations with the ratios reversed. (We number the molecular orbitals as in ref 36. I.e., the HOMO and LUMO are given the label 1; then the occupied orbitals are incremented as they decrease in energy and the virtual orbitals are incremented as they ascend in energy.) Calculations with higher excitations (doubles and triples) contribute to the **B** band, reducing its calculated transition energy and oscillator strength, but the general four-orbital picture is still generally valid, especially in its ability to describe the intensities. Table 4 shows that for both Pc structures the band labeled **Q** is comprised of approximately 90% $1a_{1u} \rightarrow 1e_g^*$ and 6% $1a_{2u} \rightarrow 1e_g^*$. This unequal mixing can be explained now by the greater $1a_{1u} - 1a_{2u}$ orbital splitting found in the Pc calculation of 0.097 eV, compared to the splitting found in the MgP complex of 0.016 eV. This leads to strongly allowed excitations into the $1e_g^*$ orbitals that are not as degenerate as in the porphyrin case and a greatly reduced configuration mixing. The transition intensities do not cancel for the lower energy band, leading to **Q** and **B** bands of nearly equal oscillator strengths, as is observed.[36] The phthalocyanine $\mathbf{B_2}$ band is composed of 63% $1a_{2u} \rightarrow 1e_g^*$ for the INDO/1 structure, while 83% of this orbital excitation is shared among the $\mathbf{B_1}$, $\mathbf{B_2}$, and **N** bands for the *ab-initio* structure. The four-orbital model still explains the origins of the Pc **Q** and **B** bands, but the strong mixing between the $1a_{1u} \rightarrow 1e_g^*$ and $1a_{2u} \rightarrow 1e_g^*$ orbital excitations found in metal porphyrins is not present in our MgPc calculation.

As can be seen from Tables 5 and 6, the **Q** band, when calculated with either structure, is approximately 1300 cm^{-1} too low in energy when compared to experiment. The **B** band is a different story; both Ough[36] *et al.* and Stillman[4] *et al.* report two close-lying bands in the region of their spectra labeled as the **B** band. Our *ab-initio* structure places two strong E_u bands within 300 cm^{-1} (4 *nm*) of each other (see Table 6), centered at 32 900 cm^{-1} (304 *nm*). A third strong E_u band lies 1500 cm^{-1} above this band pair and when plotted in Figure 2*a* forms a broad peak. We assign this peak to the observed **B** band. The INDO/1 structure places two strong E_u bands within 1300 cm^{-1} (14 *nm*) of each other centered at 31 500 cm^{-1} (318 *nm*). When plotted, this band pair also forms a broad peak (see Figure 2*b*), and we assign it to the observed **B** band.

It is of interest to note how the calculated configuration mixing and, thus, intensity vary as a function of small structural differences. The summed oscillator strengths for the **Q**−**N** bands are 6.4 for the *ab-initio* structure and 6.7 for the INDO/1 structure, or approximately the same for both structures. Inspection of Tables 5 and 6 and Figure 2 shows how the intensity is distributed between the states. Ten E_u bands lie below 45 200 cm^{-1} for both structures. Guided by their proximity and intensity, we have assigned the calculated bands to those observed. The absorption envelopes of Figure 2 both contain all the salient features of Gouterman's[35] vapor-phase MgPc spectrum, reproduced as Figure 6*a*.[38] In our

Table 6. Electronic Excitation Spectral Data for the Neutral MgPc 6-31G**-Optimized Structure

		transition energy (10^3 cm^{-1})	
state	symmetry[a]	calcd	obsd[b]
1	A_{1g}		
2, 3	E_u	13.8 (1.5504)[c] Q[d]	15.1 [15.9, 16.9][e]
4	B_{2g}	23.7	
5	A_{1g}	25.6	
6	A_{2g}	27.3	
7, 8	E_u	28.6 (0.0374)	
9	A_{2g}	30.9[f]	
13	A_{2u}	31.9[g] (0.0364)	
15, 16	E_u	32.8 (1.2856) B_1	30.3[h]
18, 19	E_u	33.1 (1.6932) B_2	
22, 23	E_u	34.4 (1.8004) N	35.7
29, 30	E_u	36.7 (0.0038)	
38, 39	E_u	38.9 (0.2190)	
43, 44	E_u	42.0 (0.1999) L	41.3
45, 46	E_u	42.8 (0.0594)	
51, 52	E_u	45.2 (1.0470) C	45.5

[a] (x, y) transforms as e_u and (z) transforms as a_{2u} in D_{4h}. [b] From ref 35. [c] Values in parentheses are calculated oscillator strengths. [d] Spectroscopic labels for the degenerate transitions, Q, B_1, B_2, N, L, and C. See ref 35. [e] Vibrational fine structure; see text, as well as refs 4 and 35. [f] The only state below 50 000 cm^{-1} with significant charge transfer character; 50% Pc → Mg ($\pi \rightarrow \pi^*$). [g] Beyond 31 900 cm^{-1} only states with calculated oscillator strengths are reported. [h] The observed band is broad (see ref 4) and is assigned to states (7−19); see also Figure 2b.

Table 7. Electronic Excitation Spectral Data for the Anion MgPc INDO/1-Optimized Structure

		transition energy (10^3 cm^{-1})	
state	symmetry[a]	calcd	obsd[b]
1	B_{2g}		
2	B_{3g}	2.89	
3	A_u	7.36 (0.0821)[c]	10.5
4	B_{1u}	8.79 (0.0063)	10.8 [11.5, 12.7][d]
5	A_u	12.3 (0.4637)	15.6
6	B_{3g}	14.6	
7	B_{1u}	15.1 (0.2313)	16.9
8	B_{2g}	18.5	
9	B_{1u}	18.8 (0.4570)	17.6
10	B_{3g}	19.9	
11	A_u	20.3 (0.1116)	18.9
12	B_{1u}	21.2[e] (0.2110)	
14	A_u	22.7 (0.0066)	
17	B_{1u}	23.5 (0.0143)	
19	B_{1u}	24.5 (0.1454)	23.4 {1}[f]
21	A_u	26.2 (0.0464)	
22	B_{1u}	26.5 (0.4601)	27.8 {2}
25	B_{3u}	27.2 (0.0003)	
29	B_{1u}	28.4[g] (0.0999)	
30	A_u	28.4 (0.0522)	
31	B_{1u}	28.6 (0.0018)	
34	A_u	29.5 (0.1246)	
35	B_{1u}	29.7 (0.1171)	
37	A_u	30.5 (0.2676)	
41	B_{3u}	31.8 (0.0316)	
44	B_{1u}	33.1 (0.0008)	
46	A_u	33.2 (0.8541)	32.3 {3}

[a] With our choice of coordinates B_{1u} is (x) allowed, A_u is (y) allowed, and B_{3u} is (z) allowed. [b] From ref 4. [c] Values in parentheses are calculated oscillator strengths. [d] See text. These are assigned as overtones of the transition observed at 10 500 cm^{-1}. [e] Beyond 21 200 cm^{-1} only states with computed oscillator strengths are reported. [f] See text. Each observed band is assigned to several calculated. See also Figure 5a. [g] The only state below 50 000 cm^{-1} with significant charge transfer character; 48% Pc → Mg ($\pi \rightarrow \pi^*$).

opinion, on the basis of the experimental results of refs 35 and 36, the calculated spectrum of the INDO/1 structure best reproduces the observed MgPc spectrum. We feel this is

Table 8. Electronic Excitation Spectral Data for the Anion MgPc 6-31G**-Optimized Structure

		transition energy (10^3 cm^{-1})	
state	symmetry[a]	calcd	obsd[b]
1	B_{2g}		
2	B_{3g}	4.93	
3	A_u	6.96 (0.1231)[c]	10.5
4	B_{1u}	9.87 (0.0037)	10.8 [11.5, 12.7][d]
5	A_u	13.9 (0.4463)	15.6
6	B_{3g}	15.4	
7	B_{1u}	15.9 (0.2255)	16.9
8	B_{2g}	19.4	
9	B_{1u}	19.6 (0.3652)	17.6
10	B_{3g}	20.6	
11	A_u	20.9 (0.1043)	18.9
12	B_{1u}	21.9[e] (0.2072)	
14	A_u	23.2 (0.0014)	
17	B_{1u}	24.0 (0.0381)	
20	B_{1u}	25.9 (0.1312)	23.4 {1}[f]
21	A_u	26.3 (0.0319)	
22	B_{3g}	27.1	
23	B_{1u}	27.6 (0.2831)	27.8 {2}
25	B_{1u}	28.2 (0.1162)	
27	A_u	29.1 (0.0025)	
29	B_{1u}	29.9[g] (0.0678)	
30	A_u	30.1 (0.0548)	
33	B_{1u}	30.9 (0.1409)	
36	A_u	32.0 (0.2151)	32.3
40	B_{1u}	33.5 (0.0562)	
41	B_{3u}	34.0 (0.0026)	
42	B_{1u}	34.1 (0.0482)	
43	A_u	34.7 (0.0137)	
47	B_{3u}	35.2 (0.0001)	
48	A_u	35.4 (0.8878)	{3}
49	A_u	35.8 (0.2839)	

[a] With our choice of coordinates B_{1u} is (x) allowed, A_u is (y) allowed, and B_{3u} is (z) allowed. [b] From ref 4. [c] Values in parentheses are calculated oscillator strengths. [d] See text. These are assigned as overtones of the transition observed at 10 500 cm^{-1}. [e] Beyond 21 900 cm^{-1} only states with calculated oscillator strengths are reported. [f] See text. Each observed band is assigned to several calculated. See also Figure 5b. [g] The only state below 50 000 cm^{-1} with significant charge transfer character; 48% Pc → Mg ($\pi \rightarrow \pi^*$).

Table 9. Allowed Prominent Bands of $MgPc^-$ as a Function of the % JT Distortion and Optimization Method (Energy, nm/10^3 cm^{-1})

INDO/1 structure		*ab-initio* structure		
D_{2h}	37% D_{2h}	D_{2h}	29% D_{2h}	expt
1359/7.36	1274/7.85	1437/6.96	1241/8.06	952/10.5
1138/8.79	1229/8.14	1013/9.87	1193/8.38	923/10.8
813/12.3	820/12.2	719/13.9	763/13.1	643/15.6
662/15.1	680/14.7	629/15.9	662/15.1	592/16.9
529/18.9	543/18.4	510/19.6	535/18.7	569/17.6
493/20.3	490/20.4	478/20.9	483/20.7	529/18.9
472/21.2	467/21.4	457/21.9	459/21.8	529/18.9
408/24.5	429/23.3	386/25.9	426/23.5	428/23.4
377/26.5	370/27.0	362/27.6	347/28.8	360/27.8
301/33.2	303/33.0	282/35.4	289/34.6	310/32.3

supported by the number of bands with appreciable intensity and their proximity to those observed experimentally; see Table 3.

It is of interest to note that one state is calculated to have appreciable charge transfer character below 50 000 cm^{-1}; it is forbidden and is of A_{2g} symmetry. For both structures this state falls at approximately 32 000 cm^{-1} and is of 50% Pc(π) → Mg-

(38) Figure 6 has been reproduced with the permission of the original references. Part a (ref 35): Copyright 1970 Academic Press. Part b (ref 4): Copyright 1992 American Chemical Society. Part c (ref 41): Copyright 1994 American Chemical Society.

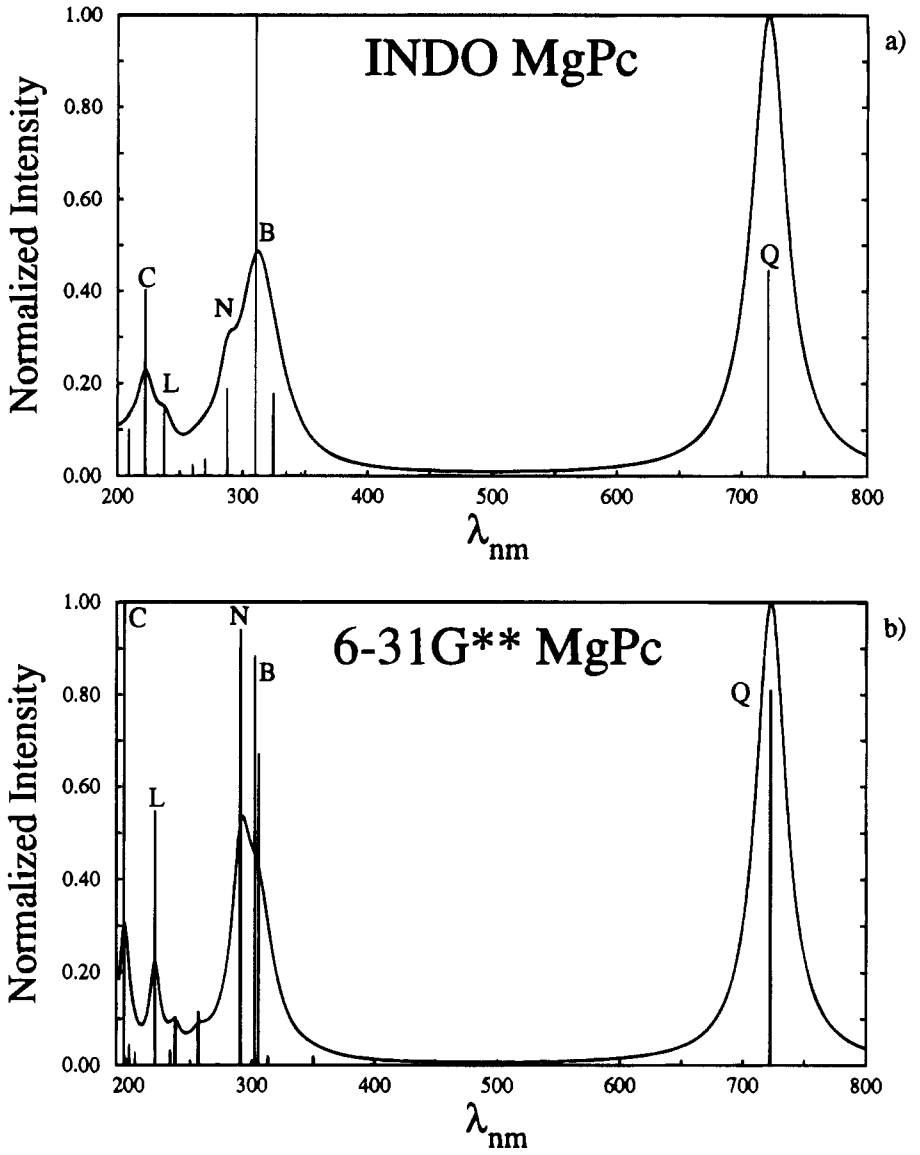

Figure 2. Calculated stick spectra for neutral MgPc: (a) for the INDO/1-optimized structure; (b) for the 6-31G**-optimized structure. The lines are broadened using a Lorentzian line shape and a width at half-height of 250 cm^{-1}; see Appendix.

(p_z) character. If populated, this state should lead to a largeMg out-of-plane displacement, as Mg^+ is a much larger ion than Mg^{2+}.[39,40]

Jahn–Teller Distortions. The LUMO of neutral MgPc is of $e_g(\pi^*)$ symmetry. Placing the reducing electron into the LUMO of the D_{4h} structure will cause the structure to undergo a first-order Jahn–Teller (JT) distortion[33] along one of the two degenerate vibrational modes, transforming as e_g. (We define the 4-fold axis to be the z axis; then the plane of the molecule defines the xy plane.) In the D_{4h} point group e_g vibrations transform as do xz and yz. Thus one expects the structure to distort along the x and y axes assuming no net out-of-plane forces, which we checked for and did not find. There are two unique choices for the x and y axes; one choice has the aza nitrogens defining these axes, and the second choice is defined by the pyrrole nitrogens. This situation is schematically shown in Figure 4.

If we choose the pyrrole nitrogens to define the x and y axes and proceed to optimize the structure via the INDO/1 or *ab-initio* methods, we obtain a structure which is a true minimum on the electronic potential energy surface. While we did not have the computational resources to compute the Hessian for such a large structure, we did though, in various ways, distort it from the computed "equilibrium" structure and in all cases upon reoptimization the structure returned to the equilibrium one. In this case the D_{4h} structure distorted with two opposing fused pyrrole–benzene groups moving closer to the central magnesium and the perpendicular pair of fused pyrrole–benzene groups moving away, with the aza nitrogens now forming the vertices of a square; i.e., the diagonals formed by connecting N_3 to N_5 and N_2 to N_4 are of equal length and are perpendicular to one another; see Table 1 and Figure 1. It was with these D_{2h} structures that we proceeded to calculate the UV–vis spectrum of the anion.

If we let the aza nitrogens define the x and y axes and proceed to optimize the structure via either method as before, we converge to an extreme point on the electronic potential energy hypersurface which has the aza nitrogens defining the vertices of a diamond structure; see Figure 4. The pyrrole nitrogens are all equidistant from the magnesium and the angles formed by N_{py}–Mg–N_{py} are 90 or 180°, where N_{py} are the pyrrole nitrogens. This is easily demonstrated to be an extreme point; displacing any one of the pyrrole nitrogens 0.005 Å away from

(39) Edwards, W. D.; Zerner, M. C. *Int. J. Quantum Chem.* **1983**, *23*, 1407.
(40) Edwards, W. D.; Head, J. D.; Zerner, M. C. *J. Am. Chem. Soc.* **1982**, *104*, 5833.

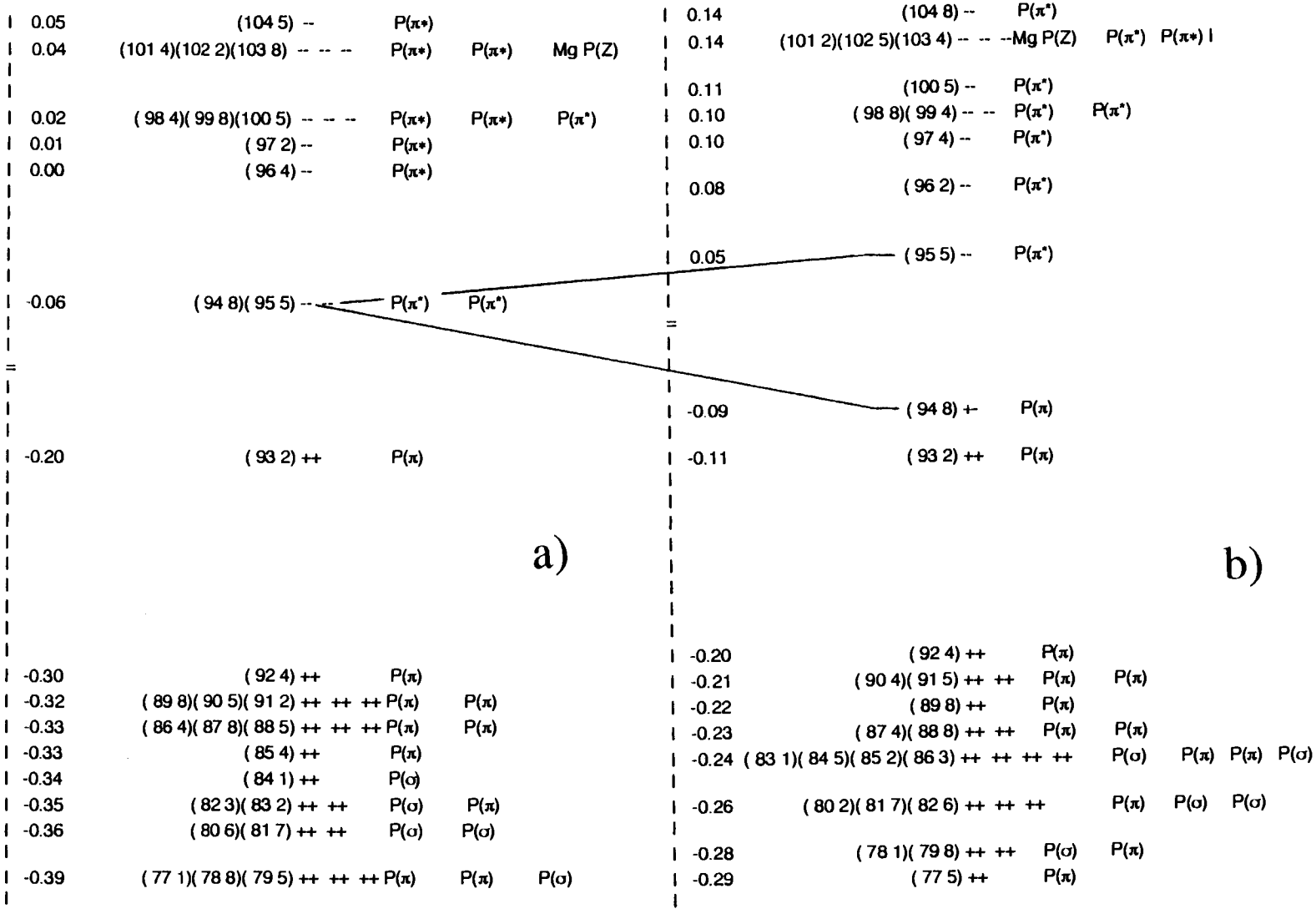

Figure 3. MO diagrams for (a) MgPc and (b) $MgPc^-$. The rightmost column is the orbital energy in eV and the (M N) label is the MO and its symmetry in the D_{2h} point group, respectively. The symmetry labels N run from 1 to 8 and are respectively A_g, A_u, B_{1g}, B_{1u}, B_{2g}, B_{2u}, B_{3u}, and B_{3g}; i.e., (12 8) would be MO $M = 12$ of symmetry B_{3g}. The rightmost columns label the orbitals as of either σ or π type.

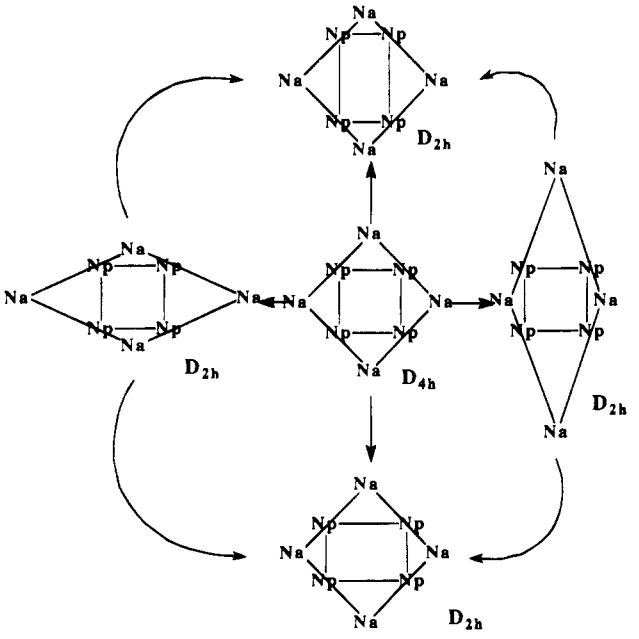

Figure 4. Symbolic representation of the possible Jahn–Teller distortions of $MgPc^-$. N_a represents the aza nitrogens and N_p the pyrrole nitrogens. The square of N_a, the top and bottom figures, are calculated to be the most stable. The four N_p then form two possible rectangles. The other two structures, the left- and rightmost figures, with the four N_a diamond-like and the four N_p square-like, represent saddle points connecting the top and bottom structures.

the Mg and reoptimizing the structure lead to the structure described in the previous paragraph. This extreme point lies 3.0 kcal/mol above the true minima for the INDO/1 structures and some 3.9 kcal/mol above the minima for the *ab-initio* structures.

As described above, the calculated anion radical structures undergo a first-order Jahn–Teller distortion to D_{2h} symmetry. The JT distortion energy for the INDO/1 structure was found to be 2600 cm^{-1}, or about 7.4 kcal/mol. This corresponds to the difference in energy between the "relaxed" anionic D_{2h} structure and the "relaxed" anionic D_{4h} structure. A fully optimized anionic *ab-initio* D_{4h} structure was computationally too expensive to obtain.

Anion Spectrum. We compare our computed spectrum to that obtained experimentally by Stillman[4] *et al.* in Figure 6*b*.[38] With our choice of coordinate system, the electronic ground state is of $^2B_{2g}$ symmetry; from this ground state the $^2B_{1u}$ states are *x*-allowed, the ^2A_u states are *y*-allowed, and the $^2B_{3u}$ states are *z*-allowed. (The molecular elongation is along the *y* axis.) The lowest lying electronic excited state of the anion, a $^2B_{3g}$ state, lies 2900 cm^{-1} above the ground state for the INDO/1 structure and 4900 cm^{-1} above for the *ab-initio* structure; it is dipole forbidden. In the molecular orbital picture of Figure 3*b* this is the OPEN → LUMO $1b_{2g}(\pi)[1e_g(\pi^*)] \rightarrow 1b_{3g}(\pi^*)$-$[1e_g(\pi^*)]$ excitation, where the bracketed symmetries relate back to the D_{4h} parentage of these orbitals. (This nomenclature has the HOMO doubly occupied and the OPEN orbital singly occupied.) The effect of reducing the molecular symmetry will, of course, split the E_u states in D_{4h} into a pair of nondegenerate states in D_{2h}, one being *x*-polarized and the other *y*-polarized. (It is obvious from Figure 6*b* how the **Q** band split.) In the region above 790 *nm* we find two dipole-allowed states. In the one-electron MO picture these are characterized as promoting an electron occupying MO 93 into MO 94, i.e. 93 → 94, and the second band is described as 93 → 95. This pair of excitations would in the neutral species be the HOMO $a_{1u}(\pi)$ into LUMO $e_g(\pi^*)$ excitation that described the **Q** band. In the anion these are the HOMO → OPEN $1a_u(\pi)[1a_{1u}(\pi)] \rightarrow 1b_{2g}(\pi^*)[1e_g(\pi^*)]$ and HOMO → LUMO $1a_u(\pi)[1a_{1u}(\pi)] \rightarrow 1b_{3g}(\pi^*)[1e_g(\pi^*)]$ excitations. We agree with Stillman[4] *et al.* that the peaks observed at 870 and 790 *nm* are vibrational overtones of the band pair described above. For both of the optimized structures we compute (1) the split **Q** band of the anion to be too low in energy by approximately 2000 cm^{-1} and (2) the splitting of the band to be too great. Experimentally the **Q** band is interpreted to be split by some 300 cm^{-1} in the anion; the INDO/1 structure gave a splitting of 1400 cm^{-1} and the *ab-initio* structure gave rise to a splitting of 3000 cm^{-1}.

We were curious as to the degree to which the anion JT distortion affects the calculated results. To investigate this, we defined a vector by the difference in geometry of the D_{4h} structure of the neutral and the D_{2h} structure of the anion and proceeded to investigate the effect on the calculated spectrum as a function of position along this vector. We found that the absolute position of the calculated bands changed only by a few hundred reciprocal centimeters and that the relative positions of the bands with respect to each other also change by, at most, a few hundred reciprocal centimeters, with two important exceptions. The splitting of the **Q** band was found very sensitive to the degree to which the structure distorted, and the band we assign to that observed at 428 *nm* was also quite sensitive to the degree of distortion; see Table 9. We found that going from the D_{4h} structure to the D_{2h} structure, we had to move 37% along the difference vector to obtain a splitting of approximately 300 cm^{-1} for the INDO/1 structure and 29% along the difference vector to obtain the same approximate splitting for the *ab-initio* structure. As noted, the absolute positions of the calculated absorptions changed by a few hundred reciprocal centimeters and for the most part shifted in the direction that improved their agreement with those experimentally observed. Those bands with parentage from the E_u bands of the D_{4h} structure move toward one another as the degree of distortion is lessened, as expected. This was most pronounced for the split **Q** band. In the one-electron MO picture the excitations describing the split **Q** band remain clean; that is, there is little mixing of other configurations into these states. As we shall see below, this is not the case for the bands that lie higher in energy; see Table 9. The computed bands in this region occur at 1360/1274 and 1138/1229 *nm* for the INDO/1 structure, and for the *ab-initio* structure they are calculated to occur at 1437/1241 and 1013/1193 *nm*. (The *first/second* notation is defined as follows: the *first* wavelength is for the fully relaxed D_{2h} structure, and the *second* wavelength is for the structure that best reproduced the **Q** band splitting.) Overall, we find that the split **Q** band of the neutral shifts to lower energy in the anion and is diminished in intensity; these reduction effects are also observed in the experimentally obtained spectrum.

In the region of the observed spectrum between 790 and 480 *nm*, there is evidence of at least four bands. These occur with maxima at about 643, 590, 569, and 530 *nm*, from Figure 6*b*. In this region, for both optimized structures, we compute five dipole-allowed bands with sufficient intensity to be easily observed. The relative intensity pattern matches that observed by Stillman *et al.*[4] (Figure 6*b*). We find two close-lying bands in the vicinity of the shoulder observed at 530 *nm* in Figure 6*b*. We feel it is probable that the shoulder observed at 530 *nm* in the $MgPc^-$ spectrum is due to these two low-intensity, close-lying bands. (The observed spectra of $MgPc^-$ and $ZnPc^-$ are remarkably similar. We find evidence of two bands forming the shoulder at 530 *nm* in the 77 K absorption spectrum of

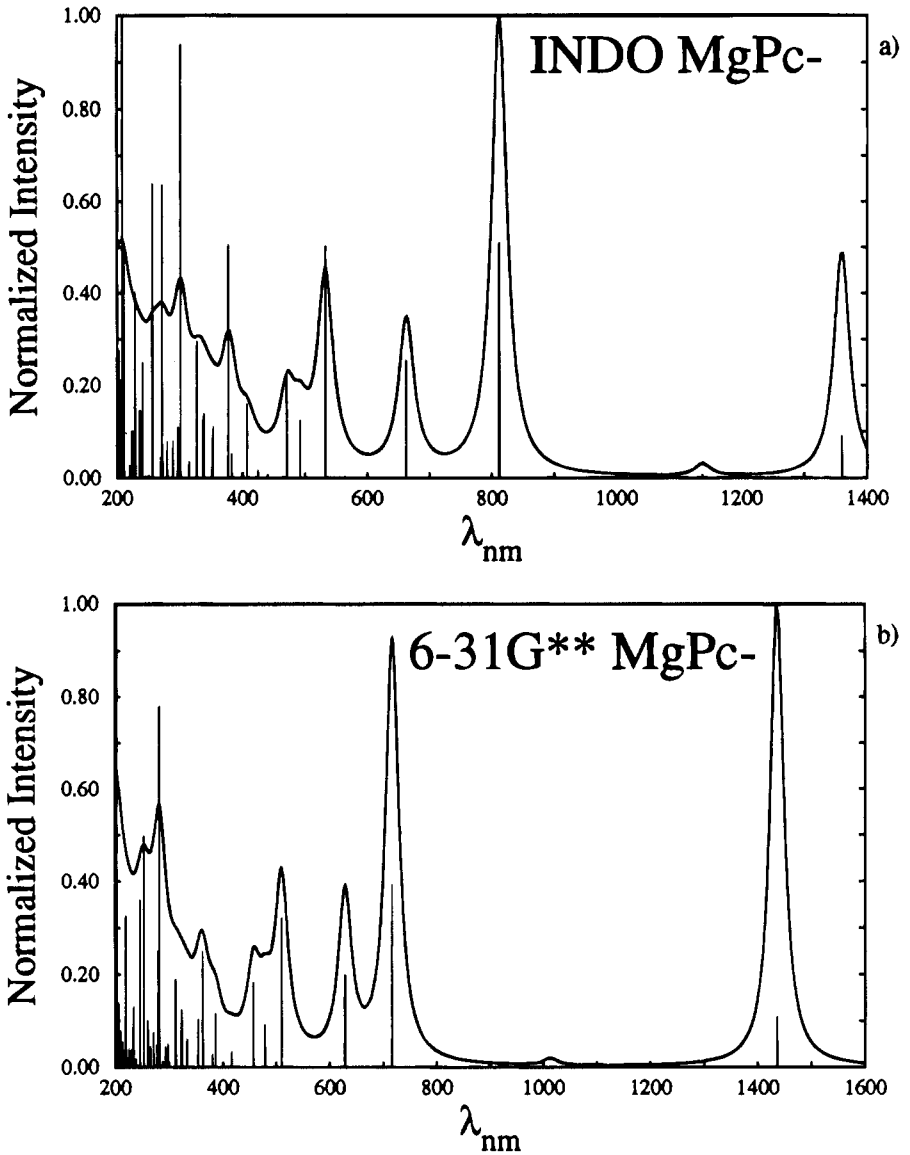

Figure 5. Calculated spectra for the MgPc anion: (a) for the INDO/1-optimized structure; (b) for the 6-31G**-optimized structure. The lines are broadened using a Lorentzian line shape and a width at half-height of 250 cm^{-1}; see Appendix.

$ZnPc^-$;[41] see Figure 6*c*.[38] Given the strong similarities between these two spectra, we feel that this lends credence to our assignment of two low-intensity bands to this shoulder.) The first of the five peaks found in this region is dominated by the 94 → 96, or the OPEN → LUMO + 1, excitation. This is the band we assign to the peak observed at 643 *nm* and we compute to occur at 812/821 *nm* for the INDO/1 structure and at 717/763 *nm* for the *ab-initio* structure. This is the last absorption band that we can assign in this manner. All calculated bands lying higher in energy are greatly mixed in the one-electron MO picture. The second band is assigned to the shoulder observed at 590 *nm* and computed at 662/678 *nm* (INDO/1) and 628/662 *nm* (*ab-initio*). The third computed band is attributed to the peak observed at 569 *nm*, which we compute to occur at 532/542 *nm* (INDO/1) and at 510/535 *nm* (*ab-initio*). The fourth and possibly fifth bands were described above. With this assignment, the average error is about 1000 cm^{-1} for the INDO/1 structure and 1200 cm^{-1} for the *ab-initio* one.

Experimentally the region below 460 *nm* is complex with several prominences. Three maxima occur at 428, 360, and 310 *nm*. In this energy range we also compute, with either structure, three comparatively intense bands. For the INDO/1 structure these occur at 407/430, 377/371, and 301/303 *nm*. In the case of the *ab-initio* structure we compute these features to occur at 386/426, 358/347, and 281/289 *nm*. The position of the band we assign to that observed at 428 *nm* is quite sensitive to the degree to which the anion JT distorts. For both structures lessening the degree of distortion, i.e. moving toward the D_{4h} structure along the difference vector, improves the agreement with experiment. From Table 9 we see that when we reproduce the **Q** band splitting, the transition energy that we associate with the 428 *nm* band is also greatly improved. Now if we group the calculated bands by their proximity to one another and their intensity, albeit guided by the observed spectrum, we generate a pattern quite similar to that observed experimentally. In Tables 7 and 8 these band groups are designated with { } and are labeled 1−3, to indicate their correspondence with the observed spectrum; we also include computed results down to 285 *nm*.

It is interesting to examine Tables 7−9 and note how the differing degree of distortion, principally of the macrocycle, affects the ordering of the states and their intensities. (A measure of how the neutral D_{4h} species distorts upon reduction, as a function of optimization method, can be found in Tables 1

(41) Mack, J.; Stillman, M. J. *J. Am. Chem. Soc.* **1994**, *116*, 1292.

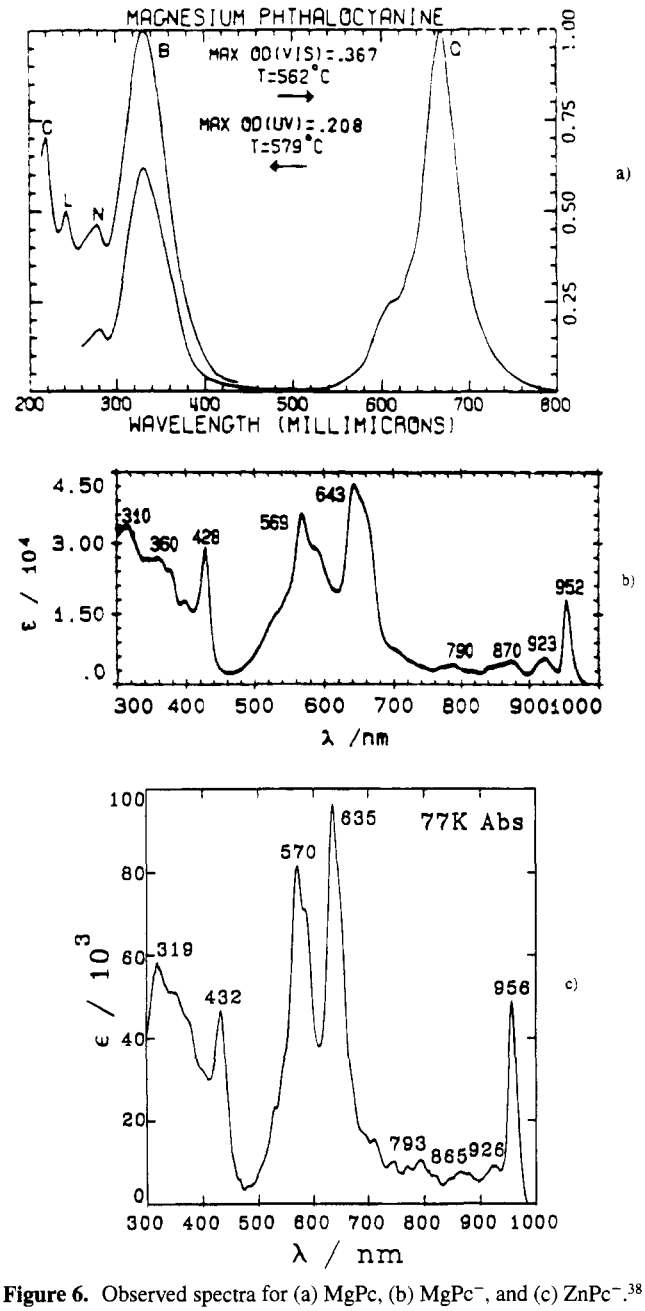

Figure 6. Observed spectra for (a) MgPc, (b) $MgPc^-$, and (c) $ZnPc^-$.[38]

and 2.) The INDO/1 structure is "more" distorted than the *ab-initio* structure for $MgPc^-$. This is easily seen from a comparison of bond angles 3−10−9 and 7−2−49 and bond lengths 1−6 and 1−19 in Tables 2 and 1, respectively. This has a pronounced effect on the calculated spectra of the anion, especially for the split **Q** band and the computed 428 *nm* peak. As is the case for the neutral, the INDO/1 structure seems to produce a calculated spectrum for the anion somewhat in better agreement with experiment than the *ab-initio* structure does.

Conclusions

While we could not compute the Hessian for either molecular species, the computed structures seem reasonable. The neutral structure is assumed to be of D_{4h} symmetry; attempts to warp the molecular plane or to displace the Mg atom out of the plane of the molecule led back to D_{4h} structures. Further, we assumed the radical anion to be of D_{2h} symmetry, and again, attempts to further reduce the symmetry of this system led back to our initial D_{2h} structure. Initial investigation on ZnPc and $ZnPc^-$ led to structures in which the Zn atom is displaced out of the plane by some 0.25 Å, as is seen experimentally.[42] At present these systems were studied at the *ab-initio* SCF level of theory using a 3-21G basis set, but our agreement with the observed ZnPc structure lends support to the methodology used in obtaining the salient features of the MgPc and $MgPc^-$ structures.

Experimentally there are five strong bands observed between 200 and 800 *nm* for the neutral gas-phase MgPc system.[35] More recent observations find that, at least, the **B** band of the gas-phase spectrum is actually two close-lying intense bands split by some 3000 cm^{-1}. We also find the **B** band of the neutral species to contain two close-lying bands. The INDO/1 structure reproduces the observed spectrum somewhat better than the *ab-initio* structure, perhaps because of a larger Mg−N distance, which is in better agreement with experiment. Additionally we find a relatively intense band, not reported experimentally, in the **L** and **C** region of the spectrum; see Figure 2. The lettered bands are described as excitations from the ground state into states of E_u electronic symmetry and are principally ($\pi \rightarrow \pi^*$) excitations localized to the macrocycle.

Our examination of the neutral MgPc spectrum, as described above, does not lead us to any conclusions that differ from those of refs 4, 35, and 36. We do predict a weak *z*-polarized band hidden under the intense band centered at 350 *nm* (see Tables 5 and 6), as well as a ligand to metal charge transfer band at 313 *nm*.

The INDO/S−CIS method has been shown in many examples[39,40,43−46] to accurately reproduce the low-energy UV−vis spectra of compounds such as these. The method consistently overestimates the **B** band of porphyrin by some 3000−5000 cm^{-1}; this also seems to be true for the phthalocyanines.

The calculated spectrum of either optimized anion structure brings into question the "goodness" of the reported structure. The improvement of the calculated spectrum, as we move along the difference vector joining the D_{2h} to the D_{4h} structure, indicates that both optimization methods may distort the molecular system to too great a degree. The dramatic improvement of the split **Q** band and the band observed at 428 *nm* as we move from D_{2h} back to D_{4h} along the difference vector demonstrates this claim, as well as the general improvement of the whole calculated spectrum. Even without the "refinement" of fitting the **Q** band splitting as a function of distortion to that observed experimentally, the calculated spectrum as a whole is good when compared to experiment.

We find that charge transfer (CT) does not seem to play an important role below 50 000 cm^{-1} for the anion; see Tables 7 and 8. For both species the CT states we do find are macrocycle to Mg charge transfer states, as would be expected for $Mg^{2+}Pc^{2-}$ and $Mg^{2+}Pc^{3-}$ molecular systems. In the case of the anion there are two states which have a one-electron character greater than 40% Pc → Mg(p_z), when the experimental **Q** band splitting is reproduced, and only one such state is present for the fully relaxed D_{2h} structure.

The four-orbital model of Gouterman does describe the origins of the **Q** and **B** bands in neutral MgPc. Unlike those of the porphyrins, the **Q** and **B** bands of magnesium phthalocyanine are not 50/50 admixtures of the $1a_{1u} \rightarrow 1e_g^*$ and $1a_{2u} \rightarrow 1e_g^*$ one-electron excitations. The pseudodegeneracy of the $1a_{1u}$ and $1a_{2u}$ orbitals found in the porphyrin does not exist for MgPc,

(42) Kobayashi, T.; Ashida, T.; Uyeda, N.; Surro, E.; Kakuda, M. *Bull. Chem. Soc. Jpn.* **1971**, *44*, 2095.
(43) Edwards, W. D.; Zerner, M. C. *Can. J. Chem.* **1985**, *63*, 1763.
(44) Edwards, W. D.; Weiner, B.; Zerner, M. C. *J. Am. Chem. Soc.* **1986**, *108*, 2196.
(45) Edwards, W. D.; Weiner, B.; Zerner, M. C. *J. Phys. Chem.* **1988**, *92*, 6188.
(46) Cory, M. G.; Zerner, M. C. *Chem. Rev.* **1991**, *91*, 813.

and this leads to a more intense **Q** band and a less intense **B** band for Pc as compared to porphyrin. For the anion, the split **Q** band is described as the $1a_{1u} \rightarrow 1e_g^*$ one-electron excitation in the neutral; for energies above those of the **Q** band, the one-electron description of the electronic excitations loses clarity and the higher energy states are described as admixtures of several such one-electron excitations. For this reason, the four-orbital model is not as complete a model for the anion as it is for the neutral.

Acknowledgment. This work was supported in part by grants from the Chisso Corp. and from the Office of Naval Research.

(47) In *Handbook of Mathematical Functions*; Abramovitz, M., Stegun, I., Eds.; Dover.

Appendix

The Lorentzian function[47] used in the plots of Figures 2 and 5 is given as

$$A(\nu) = \sum_i \sum_s \frac{2f_i}{\pi W_i \left[1 + 4\left(\frac{\nu_s - \nu_i}{W_i}\right)^2\right]}$$

where W_i is the half-height width of peak i, ν_s is the sampling frequency, ν_i is the calculated origin of peak i, f_i is the calculated oscillator strength of peak i, and the summations i and s run over all calculated bands and frequency partitions, respectively.

IC9500422